Electronic Supplementary Material (ESI) for Lab on a Chip.

Supplemental information

Joule Heating and Electroosmotic Flow in Cellular Micro/Nano Electroporation

Junjie Pan[1], Xinyu Wang[1], Chi-ling Chiang[1], Yifan Ma[3], Junao Cheng[2], Paul Bertani[2], Wu Lu[2], Ly James Lee[1]**

[1] Department of Chemical and Biomolecular Engineering, The Ohio State University, Columbus, Ohio 43210, USA

[2] Department of Electrical and Computer Engineering, The Ohio State University, Columbus, Ohio 43210, USA

[3] Department of Biomedical Engineering, The Ohio State University, Columbus, Ohio 43210, USA

* Authors to whom correspondence should be addressed. Electronic mail: lu.173@osu.edu; lee.31@osu.edu.

Table S.1. Model geometry and material parameters[1–6].

Parameter	Value
Model geometries	
Length of micron channel	200 μm
Width and height of micron well	30 μm
Length of Submicron channel	10 μm
Width and height of Submicron channel	Varies with different cases
Cell radius	7.5 μm
Membrane thickness	5 nm
Gap spacing between cell and channel	10 nm
Material electric properties	
Extracellular medium conductivity	0.8 S/m
Cytoplasm conductivity	0.2 S/m
Medium relative permeability	80
Cytoplasm permeability	80
Conductivity temporal coefficient	0.015/K
Permeability temporal coefficient	-0.005/K
Membrane conductivity	$\gg 10^{-5}$ S/m
PDMS conductivity	4×10^{-12} S/m
SiO_2 conductivity	10^{-12} S/m
SiO_2 zeta potential	-0.02 V
PDMS zeta potential	-0.02 V
Material thermal properties	
Medium conductivity	0.6 W/m K
Whole cell thermal conductivity	0.6 W/m K
PDMS thermal conductivity	0.15 W/m K
SiO_2 thermal conductivity	1.3 W/m K

Discussion on simulation with and without involving PDMS and SiO_2 sidewalls.

In the simulation, the heat loss to the surroundings and the dynamic heat balance is taken into consideration. The model was calibrated to match the experimental results in general (**Fig.4b**). Without considering the PDMS device, simulation results could show significant discrepancy to the experimental data. Two extreme situations can be compared with. First, the fluid and device interface all have thermal insulation boundary conditions. Then, the heat dissipation to the surroundings could be greatly underestimated and the heat increase in the fluids could be unreasonably fast and the natural cooling down process unreasonably slow. Second, natural convection or constant temperature boundary conditions can be applied to the interface between fluid and sidewalls. In this case, the heat dissipation to the surroundings could be overestimated and we could hardly observe much temperature oscillation between pulse to pulse.

The real situation lies in between these two extreme conditions. Only by involving the PDMS-SiO_2 device in the analysis, we can reproduce the following effect that we observed experimentally. First, significant temperature increase (in a range between from room temperature to water boiling point) induced by the heat generation inside the small channel. Second, the fast cooling of the cell between pulses (with 0.1s pulse interval) (**Fig.3c** and **Fig.4b**). After a 10-pulse electroporation within 1 s, we observed the whole cell cooled down to room temperature within 1s (**Fig.4b**). Therefore, both PDMS and SiO2 sidewall has to be incorporated into the model so that we can successfully match the simulation results with the experimental observation (**Fig.4b**). And then draw the following conclusion from there.

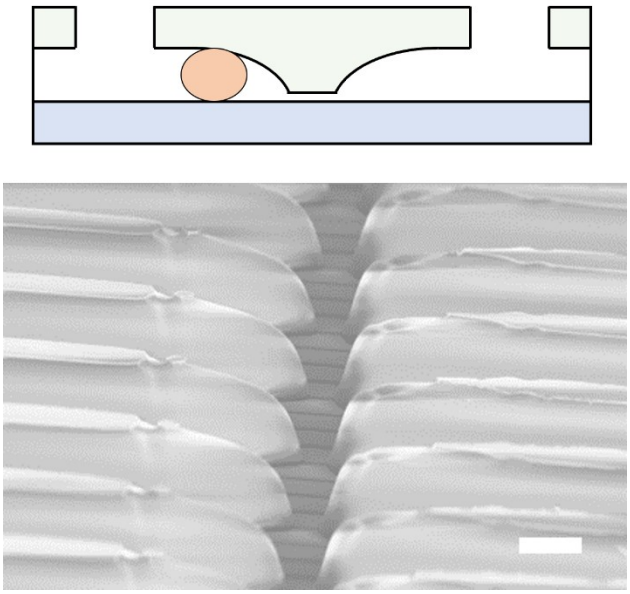

Figure S1. SEM image of SPR220's patterned micro wires. They have non-vertical side walls, tapered ends, and poor uniformity. In some cases, cells can't be trapped to the outlet of the nanochannel. Large gap spacing is not good for NEP/MEP use.

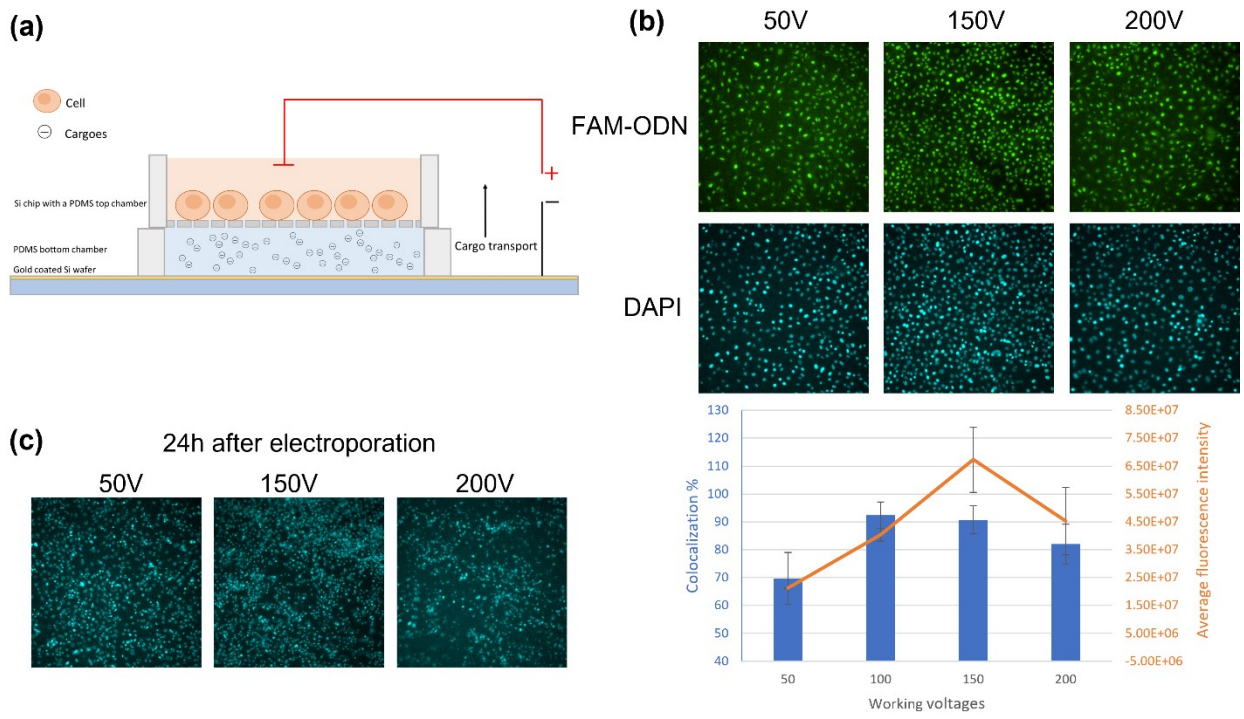

Figure S2. Cell transfection in 3D NEP. **(a)** Experimental setup of 3D NEP. Cells stand on a porous substrate and cargo solution in the reservoir beneath the porous substrate. The Si substrate has a well-defined nanopore arrays as reported in our previous study[7,8]. **(b)** Transfection voltage scan from 50 V to 200 V for FAM-ODN delivery. The percentage of the transfected cells is defined by colocalization %, the green-fluorescent cells (GFP) per total number of cells (DAPI). The average fluorescence intensity of the cell is defined by total fluorescence intensity of the image/total number of cells. The transfection% peaks at 100 V and the average transfection dose peaks at 150V. Both decrease with increasing voltage. **(c)** cell viability 24 hrs after NEP. With increasing voltage, cell viability decreases, and more cells are detached from the substrates.

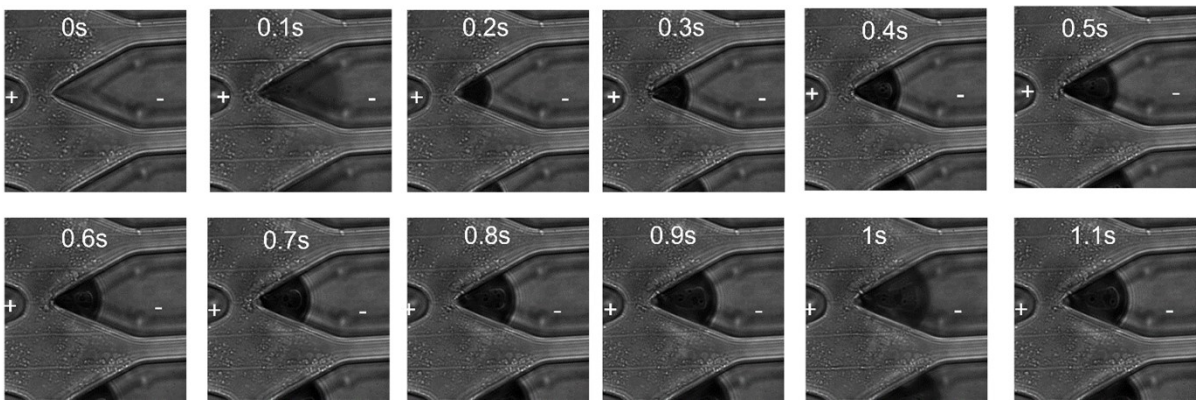

Figure S3. Bubble formation in an extreme situation (250V, no cell loaded in the microchannel). The positive electrode is placed on the far left and negative electrode on the far right. A large gas bubble is observed on the right outlet of the nanochannel, and its size increases during pulsing.

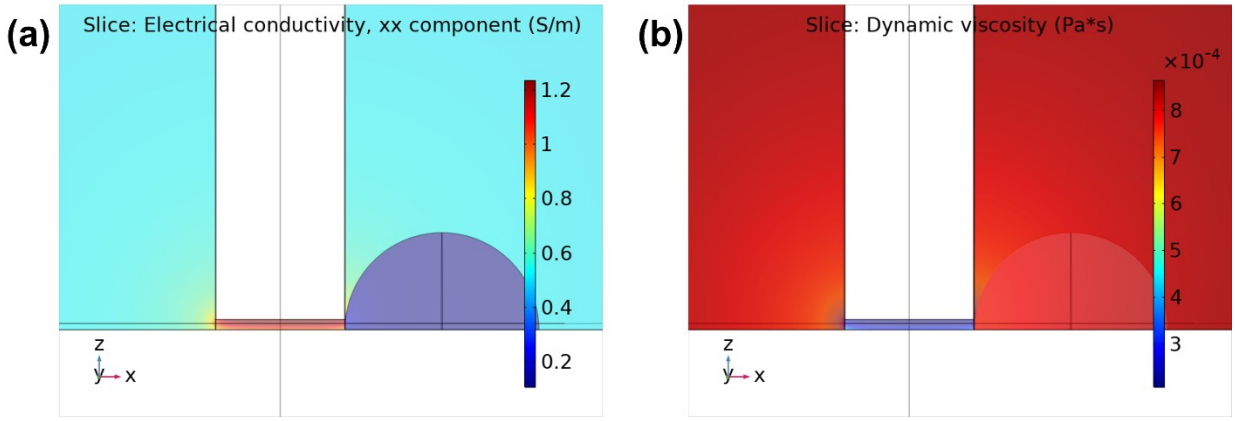

Figure S4. Heterogenous material properties in the 3D dimension during electroporation**. (a)** electric conductivity of the fluid and cytosol. **(b)** fluid viscosity. Due to the high local temperature inside the nanochannel, the fluid has higher electrical conductivity and lower viscosity.

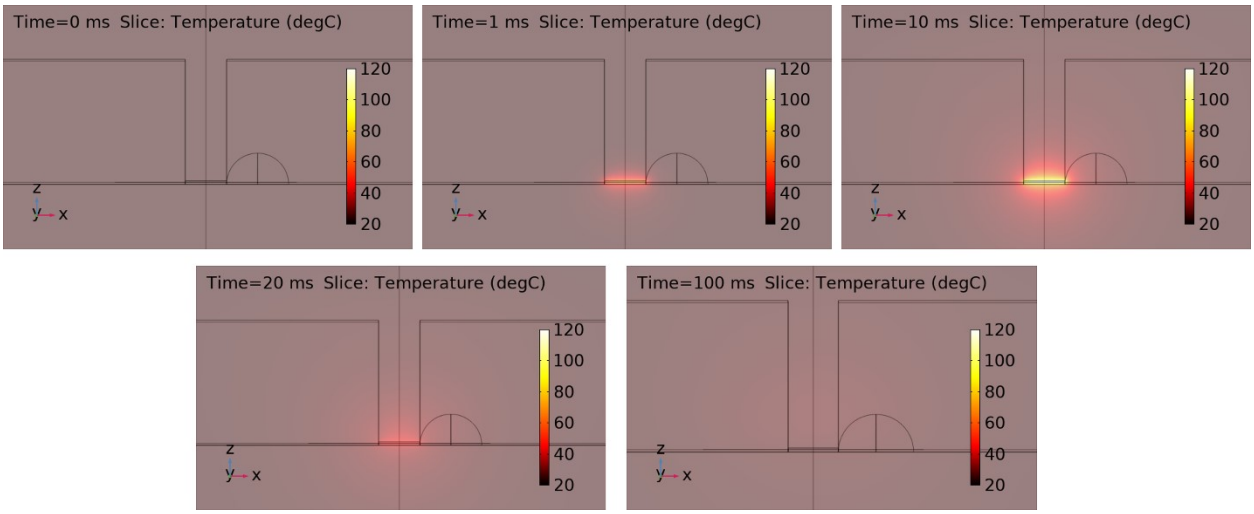

Figure S5. Dynamic temperature changes during and after electroporation (square wave pulse: 150 V, 0-10 ms).

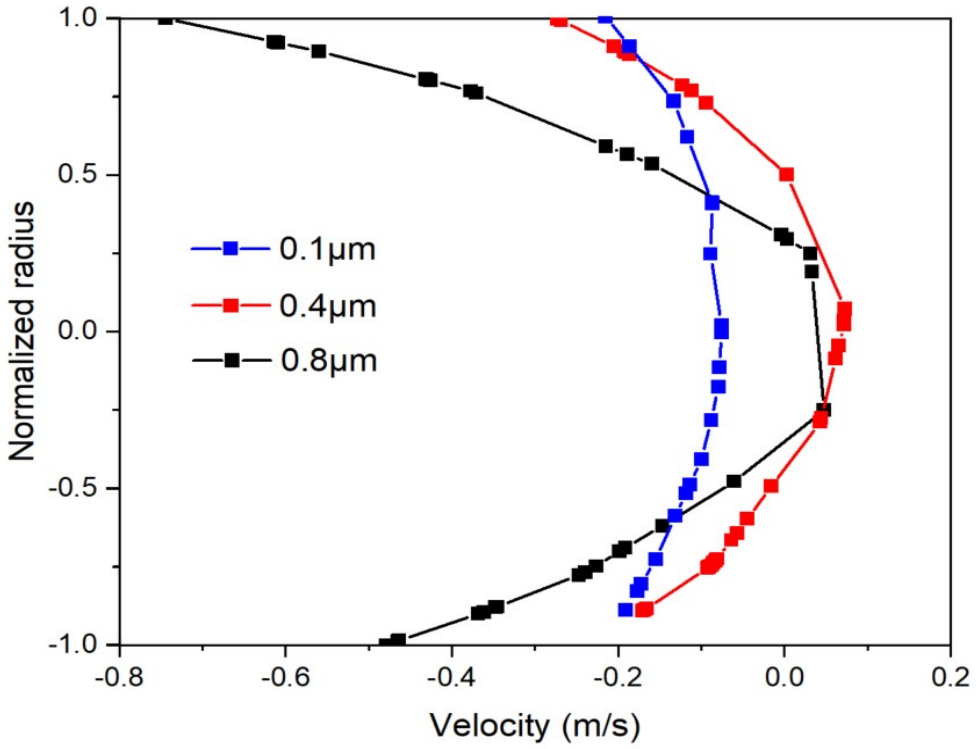

Figure S6. Velocity profile in different sized channels (transfection voltage = 150 V).

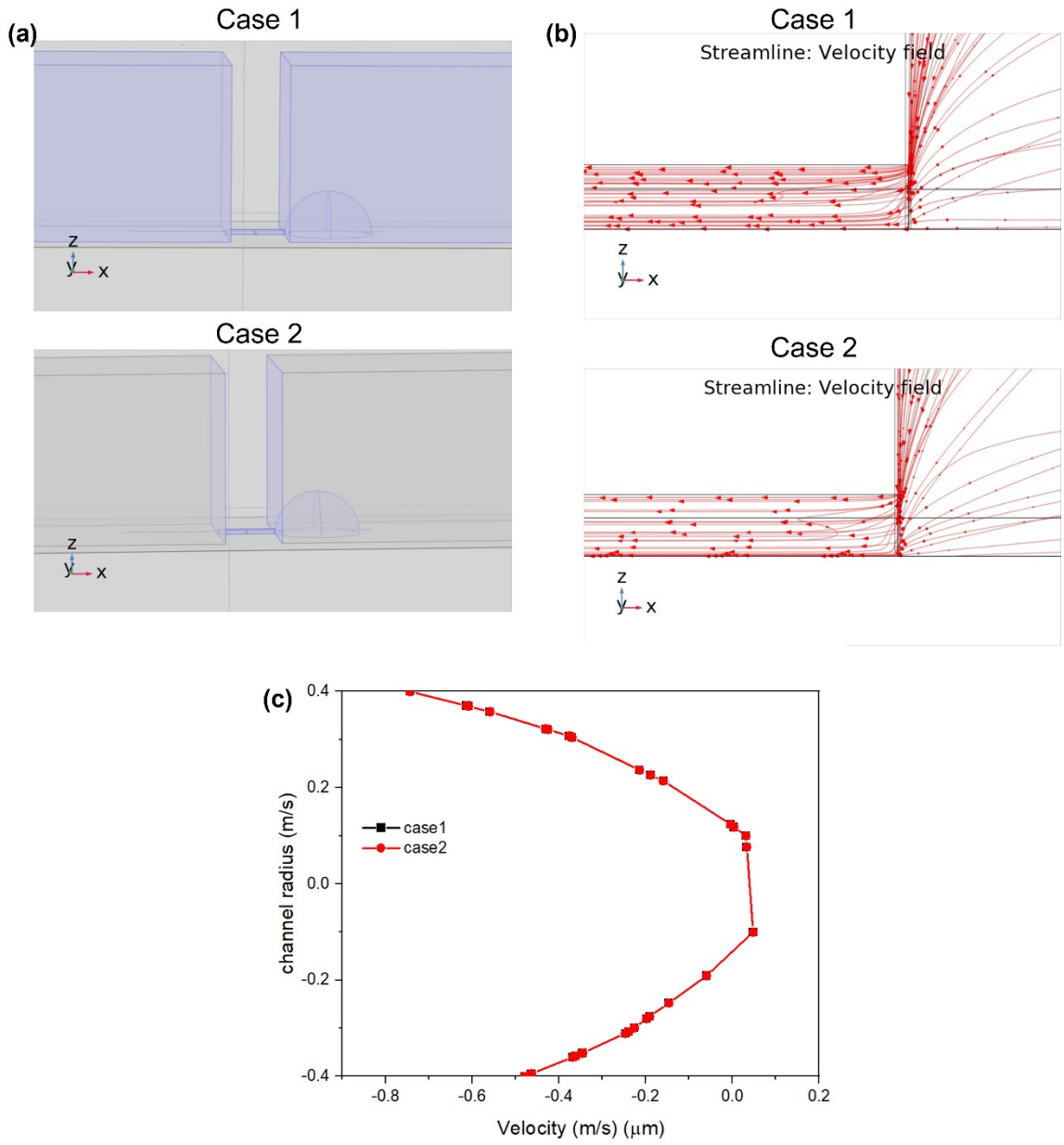

Figure S7. Fluid field simulation between the two cases. **(a)** case 1 for the device in this work: gravity in -z direction. All sidewalls are negatively charged. Case 2 for mimicking the NEP using porous substrates: gravity in -x direction. Part of the sidewalls are negatively charged. **(b) and (c)** no significant difference between the flow fields and velocity profiles in both case 1 and 2.

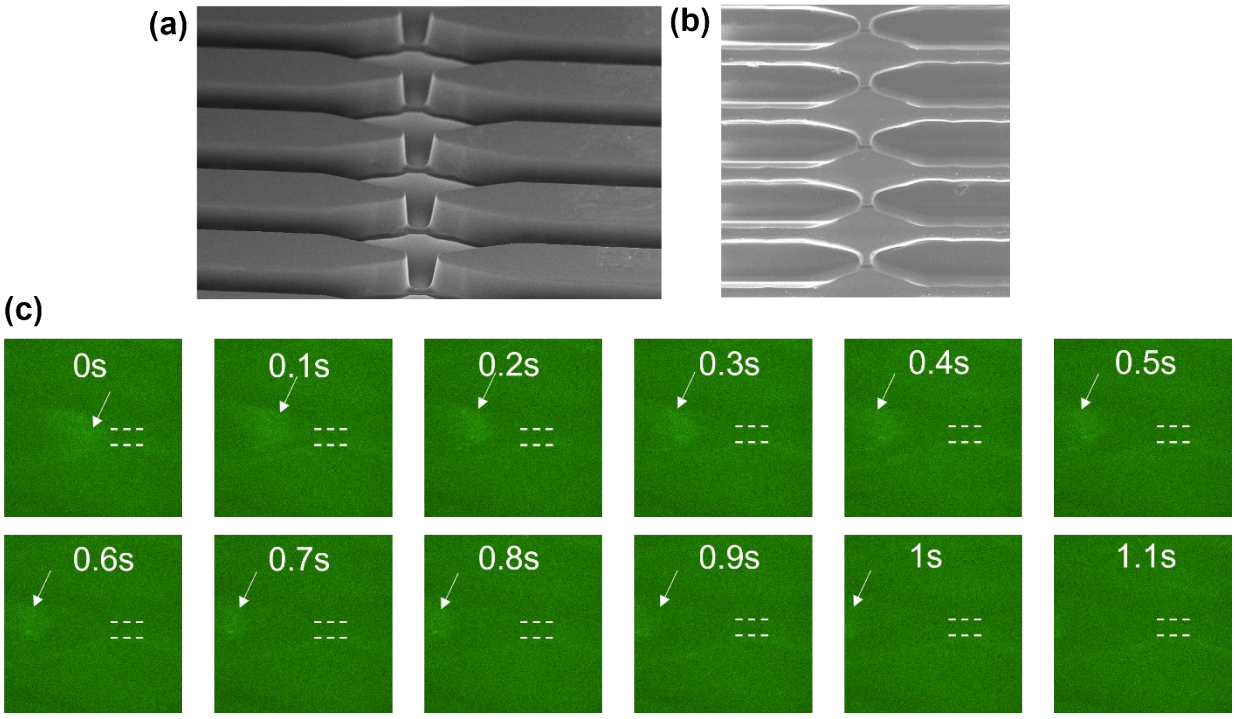

Figure S8. **(a)** fabrication of the Si master with a channel size of 5 μm. **(b)** Cell being pushed out away from the microchannel when 80 V transfection voltage is applied. This agrees with the simulation results shown in **Fig 4(f)**.

References

(1) Liao, W.-C. Single DNA Dynamics and Cell Electroporation in Micro/Nanofluidics, The Ohio State University, 2012.

(2) Prabhakaran, R. A.; Zhou, Y.; Patel, S.; Kale, A.; Song, Y.; Hu, G.; Xuan, X. Joule Heating Effects on Electroosmotic Entry Flow. *ELECTROPHORESIS* **2017**, *38* (5), 572–579. https://doi.org/10.1002/elps.201600296.

(3) Kyoo Park, B.; Yi, N.; Park, J.; Kim, D. Thermal Conductivity of Single Biological Cells and Relation with Cell Viability. *Appl. Phys. Lett.* **2013**, *102* (20), 203702. https://doi.org/10.1063/1.4807471.

(4) Wang, J.; Zhu, W.; Zhang, H.; Park, C. B. Continuous Processing of Low-Density, Microcellular Poly(Lactic Acid) Foams with Controlled Cell Morphology and Crystallinity. *Chemical Engineering Science* **2012**, *75*, 390–399. https://doi.org/10.1016/j.ces.2012.02.051.

(5) Pan, J.; Chiang, C.-L.; Wang, X.; Bertani, P.; Ma, Y.; Cheng, J.; Talesara, V.; Ly James, L.; Wu, L. Cell Membrane Damage and Cargo Delivery in Nanoelectroporation. *Nanoscale* **2023**. https://doi.org/10.1039/D2NR05575A.

(6) Song, L.; Yu, L.; Brumme, C.; Shaw, R.; Zhang, C.; Xuan, X. Joule Heating Effects on Electrokinetic Flows with Conductivity Gradients. *ELECTROPHORESIS* **2021**, *42* (7–8), 967–974. https://doi.org/10.1002/elps.202000264.

(7) Chang, L.; Bertani, P.; Gallego-Perez, D.; Yang, Z.; Chen, F.; Chiang, C.; Malkoc, V.; Kuang, T.; Gao, K.; Lee, L. J.; Lu, W. 3D Nanochannel Electroporation for High-Throughput Cell Transfection with High Uniformity and Dosage Control. *Nanoscale* **2016**, *8* (1), 243–252. https://doi.org/10.1039/C5NR03187G.

(8) Bertani, P.; Lu, W.; Chang, L.; Gallego-Perez, D.; James Lee, L.; Chiang, C.; Muthusamy, N. Bosch Etching for the Creation of a 3D Nanoelectroporation System for High Throughput Gene Delivery. *Journal of Vacuum Science & Technology B, Nanotechnology and Microelectronics: Materials, Processing, Measurement, and Phenomena* **2015**, *33* (6), 06F903. https://doi.org/10.1116/1.4932157.